PAPER I

The Institution of Electrical Engineers

Founded 1871 Incorporated by Royal Charter 1921

This is to certify that for the session
1995/1996 the Council have awarded

THE IERE BENEFACTORS PREMIUM

to

M A Briffa
Dr M Faulkner

for the paper entitled

"Stability analysis of Cartesian feedback linearisation for amplifiers with small nonlinearities"

Witness our hands and seal at Westminster
this 30th day of September 1997

President

Member of Council

Secretary

Stability analysis of Cartesian feedback linearisation for amplifiers with weak nonlinearities

M.A. Briffa
M. Faulkner

Indexing terms: Linearisation, RF amplification, Cartesian feedback, Intermodulation

Abstract: RF amplifier linearisation by Cartesian feedback is analysed using a multiple input multiple output (MIMO) model. The effects of RF amplifier distortion, namely AM/AM and AM/PM distortion, are shown to degrade the stability of the Cartesian feedback loop. A versatile technique is presented that allows the amount of stability degradation to be determined for RF amplifiers provided distortion is not too large (i.e class A to class AB amplifiers). Loops with low stability margins are shown to exhibit out-of-band noise peaking. It is concluded from the noise analysis undertaken, that the highest proportion of gain possible should be placed ahead of the loop compensation to minimise out-of-band noise.

1 Introduction

The combined use of amplitude and phase modulation delivers the improved spectral efficiency of so-called linear modulation schemes. Such schemes however, can undergo significant distortion when amplified by efficient yet nonlinear amplifiers. This distortion is caused by the amplitude variations of the signal and is composed of AM/AM and AM/PM components. As a result, the previously compact spectrum is broadened into adjacent channels and the signal is made harder to detect thus degrading the BER.

The traditional Class A/back-off approach of linear amplification has poor efficiency and is therefore impractical for portable wireless transmitting applications and less attractive for use in power conscious basestations. Consequently, various linearisation strategies have been devised which exploit the efficiency of nonlinear amplifiers by reducing their distortion to acceptable levels. These linearisation strategies can be summarised as embracing predistortion (fixed or adaptive) [1], constant envelope vector summation (e.g. LINC and CALLUM [2]), feedforward [3] or feedback techniques [4].

Feedback has long been used to linearise nonlinear systems. Cartesian feedback linearisation, as illustrated in Fig. 1, compares the baseband Cartesian inputs with the baseband Cartesian signals demodulated from the output and presents the RF amplifier with the predistorted drive necessary to achieve linearisation.

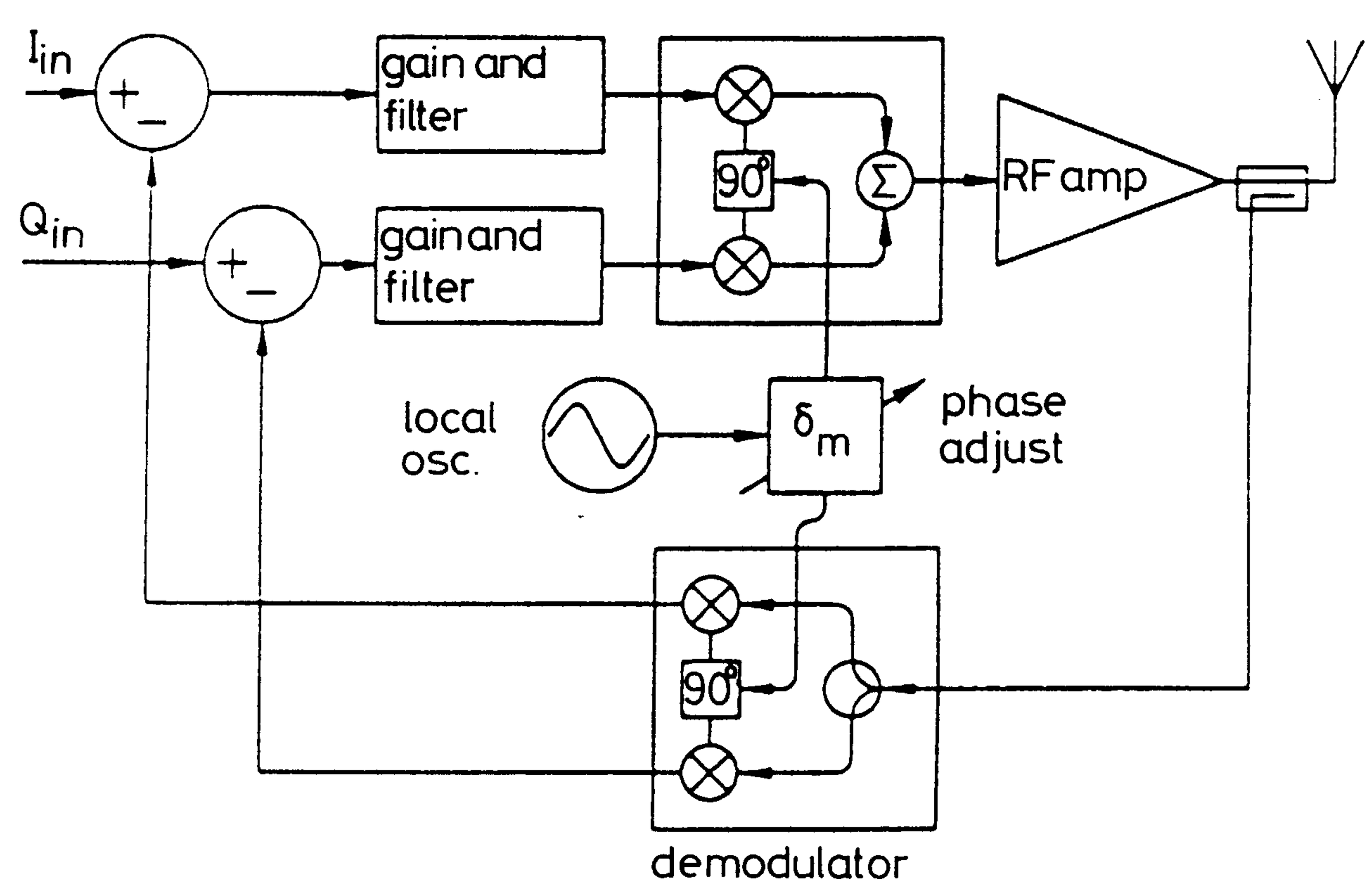

Fig. 1 *Cartesian feedback transmitter*

The loop control characteristics are established by the gain and the compensation filters. The level of intermodulation distortion reduction is essentially governed by the loop gain, and the compensation allows the stability and behaviour of the system to be controlled.

Synchronism between the modulator and demodulator is obtained by splitting a common RF carrier. Due to RF path differences in the forward and feedback paths, a phase adjuster (δ_m) is necessary to maintain the correct relationship between the input signals and feedback signals. The setting of this adjuster and how the RF amplifier nonlinearities influence this setting is discussed in this paper. Further aspects of Cartesian feedback are also covered in [5–7].

In common with other closed feedback loops, however, this technique is only conditionally stable. Prior to instability, the noise floor of the Cartesian feedback loop tends to rise at the least stable frequencies. So, in addition to stability constraints, out-of-band noise performance of the Cartesian feedback loop is also examined in this paper.

2 MIMO modelling of Cartesian feedback

Stability will be assessed by considering the amplifier's response to a small perturbation signal ΔV_i, about an operating point set by the input vector V_i. The model is

© IEE, 1996

IEE Proceedings online no. 19960614

Paper first received 15th July 1994 and in revised form 21st February 1996

M.A. Briffa was with Victoria University of Technology, Australia and is now with Ericsson Radio Access AB, PO Box 11, S-164 93 Stockholm, Sweden

M. Faulkner is with the Mobile Communications and Signal Processing Group, Department of Electrical and Electronic Engineering, Victoria University of Technology, PO Box 14428 MCMC, Melbourne VIC 8001, Australia and is Visiting Professor, Department of Applied Electronics, Lund University, Sweden until 1997

first simplified by moving the bulk RF phase rotation which exists between the forward and feedback paths, into a separate block as shown in Fig. 2. This allows the input and output vectors to be shown in phase with each other (Figs. 3*a–d*). Using the input vector V_i as the reference for the co-ordinate system defines:

$$\Delta v_i = \Delta a + j\Delta b \tag{1}$$

where Δa is in phase with V_i and Δb is orthogonal to V_i (Fig. 3*a*).

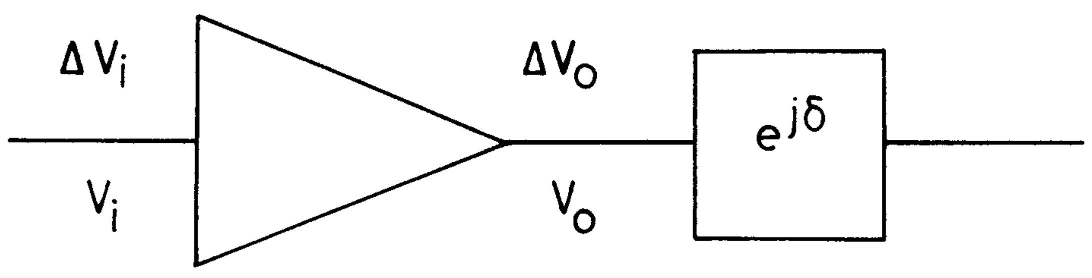

Fig.2 *RF amplifier representation with bulk RF rotation separated*

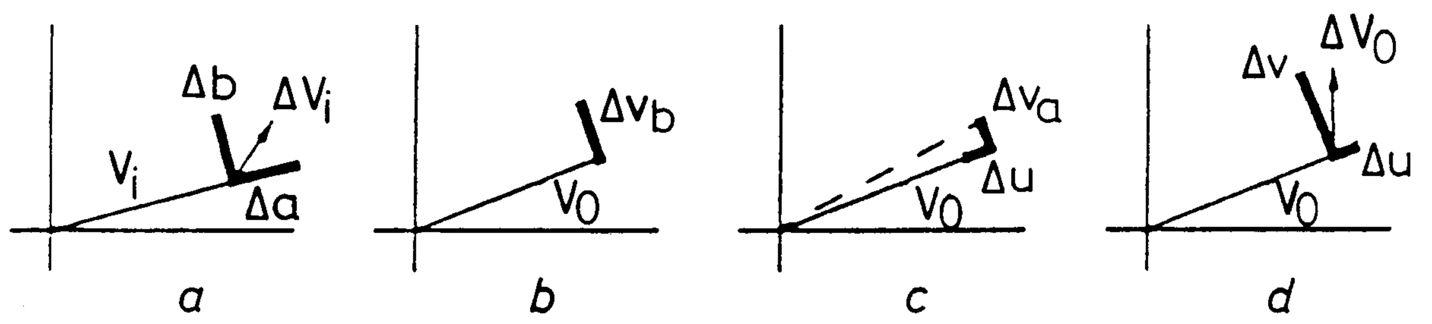

Fig.3 *Signals and perturbations as they pass through RF amplifier*
a Input signal and corresponding applied input perturbation
b Output signal with perturbation caused by phase change on input vector
c Output signal with perturbations caused by amplitude change on input vector
d Output signal with total output perturbation

The effect of Δb is to produce a phase change in the input vector (no amplitude change), and a corresponding phase change in the output vector only, hence, the resulting output perturbation Δv_b (Fig. 3*b*) is

$$\Delta v_b = \frac{|V_o|}{|V_i|}\Delta b = g_q \Delta b \tag{2}$$

where g_q is the large signal gain.

The foremost effect of Δa is to increase the amplitude of V_0 by the differential gain, g_i

$$\Delta u = \frac{\Delta|V_o|}{\Delta|V_i|}\Delta a = g_i \Delta a \tag{3}$$

The change in the input and hence output amplitude also causes a change in the phase (AM to PM effect) and hence an orthogonal component Δv_a is also generated (Fig. 3*c*)

$$\Delta v_a = \frac{|V_o|\Delta\angle V_o}{\Delta|V_i|}\Delta a = |V_o| g_d \Delta a \tag{4}$$

where g_d is the slope of the phase curve. The resulting output perturbation is then defined as (Fig. 3*d*)

$$\Delta v_o = \Delta u + j(\Delta v_a + \Delta v_b) = \Delta u + j\Delta v \tag{5}$$

The full model for the perturbation gain of the amplifier is summarised in Fig. 4.

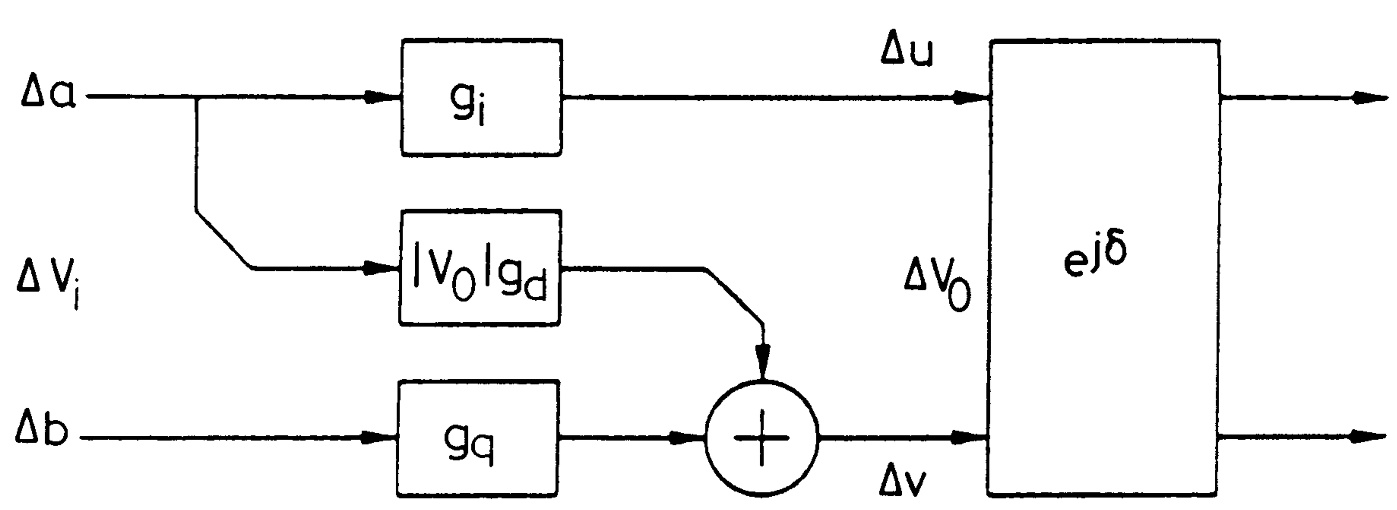

Fig.4 *Full perturbation model of RF amplifier with bulk RF rotation separated*

Simplifications to the model can be justified for certain types of amplifiers. The cross-coupling term $|V_0|g_d$ can be neglected if this is appreciably lower than the g_i and g_q gains. Also, if the difference between g_i and g_q is small, they can be replaced by a single gain term g. These conditions apply to amplifiers with low turn-on distortion (class A and AB) and operating below compression. Fig. 11 shows g_i, g_q and $|V_0|g_d$ plotted against V_i for the class AB amplifier in this paper (Figs. 9 and 10). The above conditions hold for input levels up to just below the 1dB compression point (solid lines). Finally, Fig. 12 combines the plots of Figs. 10 and 11 to show the amplifier phase shift as a function of amplifier gain. This plot will be used later in this paper.

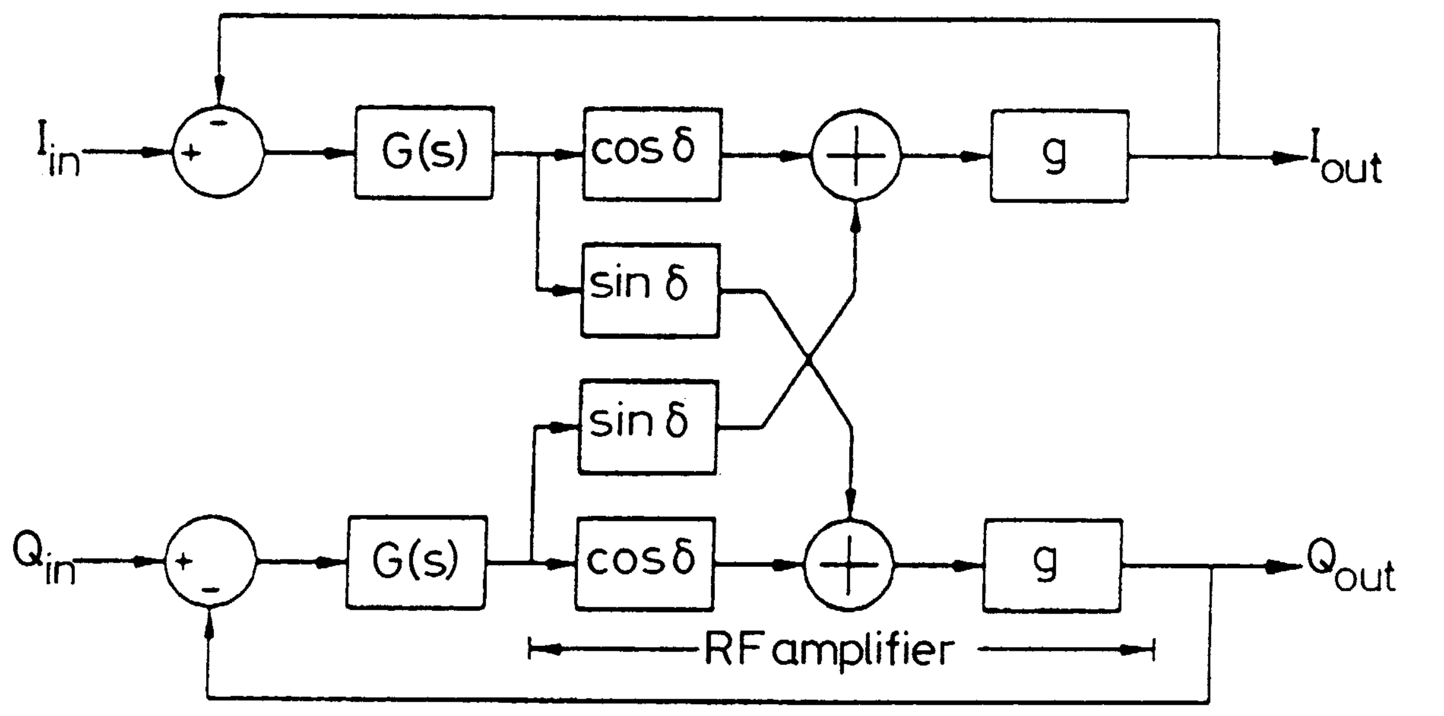

Fig.5 *MIMO representation of Cartesian loop with simplified linear RF amplifier model*

Once this simplified RF amplifier model is defined, it is possible to investigate stability by using a multiple input multiple output (MIMO) model of the Cartesian feedback loop (Fig. 5). The RF amplifier is represented as a general block with a gain (g) and an RF phase difference (δ). In a perfectly linear amplifier these parameters would be constant with changes in power levels, carrier frequency, temperature, and time. In most power efficient amplifiers however, the gain and the RF phase difference are usually level dependent and variable. A piecewise stability analysis is used in this paper to accommodate the changes in the amplifier characteristics (g and δ) which do exist. It has also been assumed in this paper that the amplifier is wide-band compared to the loop filtering and modulation and so frequency dependence of the RF amplifier parameters has been neglected. The modulator and demodulator were assumed to be ideal and the controller function $G(s)$ replaces the gain and filter blocks of Fig. 1.

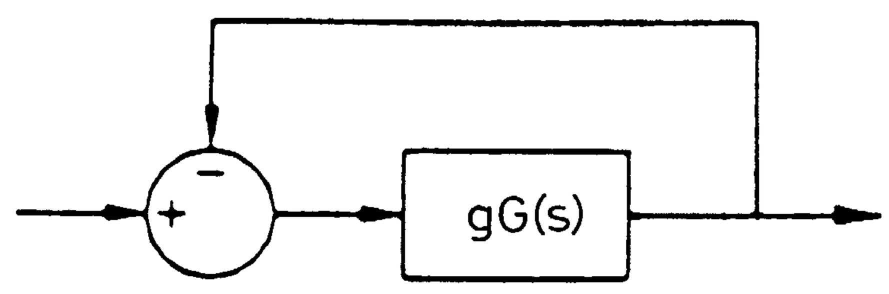

Fig.6 *Stability model when $\delta = 0$*

When the phase difference $\delta = 0$, the model of Fig. 5 can be simplified to that shown in Fig. 6. The stability of this system can be described using traditional control theory through the gain and phase margin of the $gG(s)$ function.

The analysis in this paper holds for amplifiers whose absolute gain (output voltage/input voltage) is approximately equal to the differential gain (change in output voltage/change in input voltage), and whose rate of change of RF phase difference is small over the operating range as discussed above. This includes most amplifiers operating between class A to class AB, but excludes amplifiers with significant turn-on distortion such as class C. The linearisation of amplifiers with weak nonlinearities is necessary in systems where the intermodulation distortion performance is strict (e.g. PMR; –70dB in adjacent channel). This is because the cost-effective improvement that linearisation techniques can provide is generally limited, which implies that the raw unlinearised amplifier must be reasonably linear to start with.

2.1 Effects of amplifier characteristics on stability I

In matrix form the open loop transfer function described by the model is given by

$$\begin{bmatrix} \cos\delta & -\sin\delta \\ \sin\delta & \cos\delta \end{bmatrix} \begin{bmatrix} g & 0 \\ 0 & g \end{bmatrix} \begin{bmatrix} G(s) & 0 \\ 0 & G(s) \end{bmatrix} = \begin{bmatrix} gG(s)\cos\delta & -gG(s)\sin\delta \\ gG(s)\sin\delta & gG(s)\cos\delta \end{bmatrix} \quad (6)$$

Instability results whenever the following condition (the characteristic equation of the closed loop system) is satisfied:

$$\left| I + \begin{bmatrix} gG(s)\cos\delta & -gG(s)\sin\delta \\ gG(s)\sin\delta & gG(s)\cos\delta \end{bmatrix} \right| = 0 \quad (7)$$

where the absolute symbolises the determinant of a matrix, and I is the identity matrix.

If instability occurs in the system, it will occur at some frequency which implies the frequency dependent function of $G(s)$ will be equivalent to some complex number. Combining $G(s)$ and g and setting this product to some complex number G reduces eqn. 7 to

$$G^2 + 2G\cos\delta + 1 = 0 \quad (8)$$

The solution to eqn. 8 for G is given by

$$G = \frac{-2\cos\delta \pm \sqrt{4\cos\delta^2 - 4}}{2} \quad (9)$$

This solution is complex since the expression within the square root is negative or zero. G is therefore given by:

$$G = \frac{-2\cos\delta}{2} \pm j\frac{\sqrt{4 - 4\cos\delta^2}}{2} = -\cos\delta \pm j\sin\delta \quad (10)$$

Since the magnitude of $gG(s)$ is one at the frequency where its phase margin is measured (Fig. 6), it follows that the angle of eqn. 10 is related to the phase margin of $gG(s)$ by

$$\angle(gG(s)) = \angle(-\cos\delta \pm j\sin\delta)$$

$$\Rightarrow \pm(\text{phase margin of } [gG(s)] - \pi) = \pm(|\delta| - \pi) \quad (11)$$

$$\therefore \text{phase margin of } [gG(s)] = pm_G = |\delta|$$

The amount of RF phase rotation (δ) which can be tolerated before instability results will be termed δm_G and is

$$\delta m_G = pm_G - |\delta| \quad (12)$$

Stability is insured provided δm_G remains positive. Instability occurs ($\delta m_G \leq 0$) whenever the amount of RF phase rotation completely consumes the phase margin of $gG(s)$. Note, however, that this does not indicate that RF phase rotation and baseband phase shift are equivalent.

2.2 The difference between RF phase rotation and baseband phase shift

RF phase rotation causes cross-coupling whereas baseband phase shift results is a phase shift in a time sense. The difference is best demonstrated in Fig. 7. The solid line represents the phase shift as a function of positive and negative frequency for a first order transfer function given by $G(s)$ which is equated to a transfer function consisting of a single pole p at a pole location frequency given in radians per second, a DC gain term K and a time delay τ given in seconds:

$$G(s) = \frac{K_p}{s + p} e^{-\tau s} \quad (13)$$

The use of a delay allows phase shift introduced by high frequency poles and zeros to be modelled along with actual transmissive delay. The graphs were obtained by taking the double-sided FFT (fast Fourier transform) of the impulse response of the transfer function.

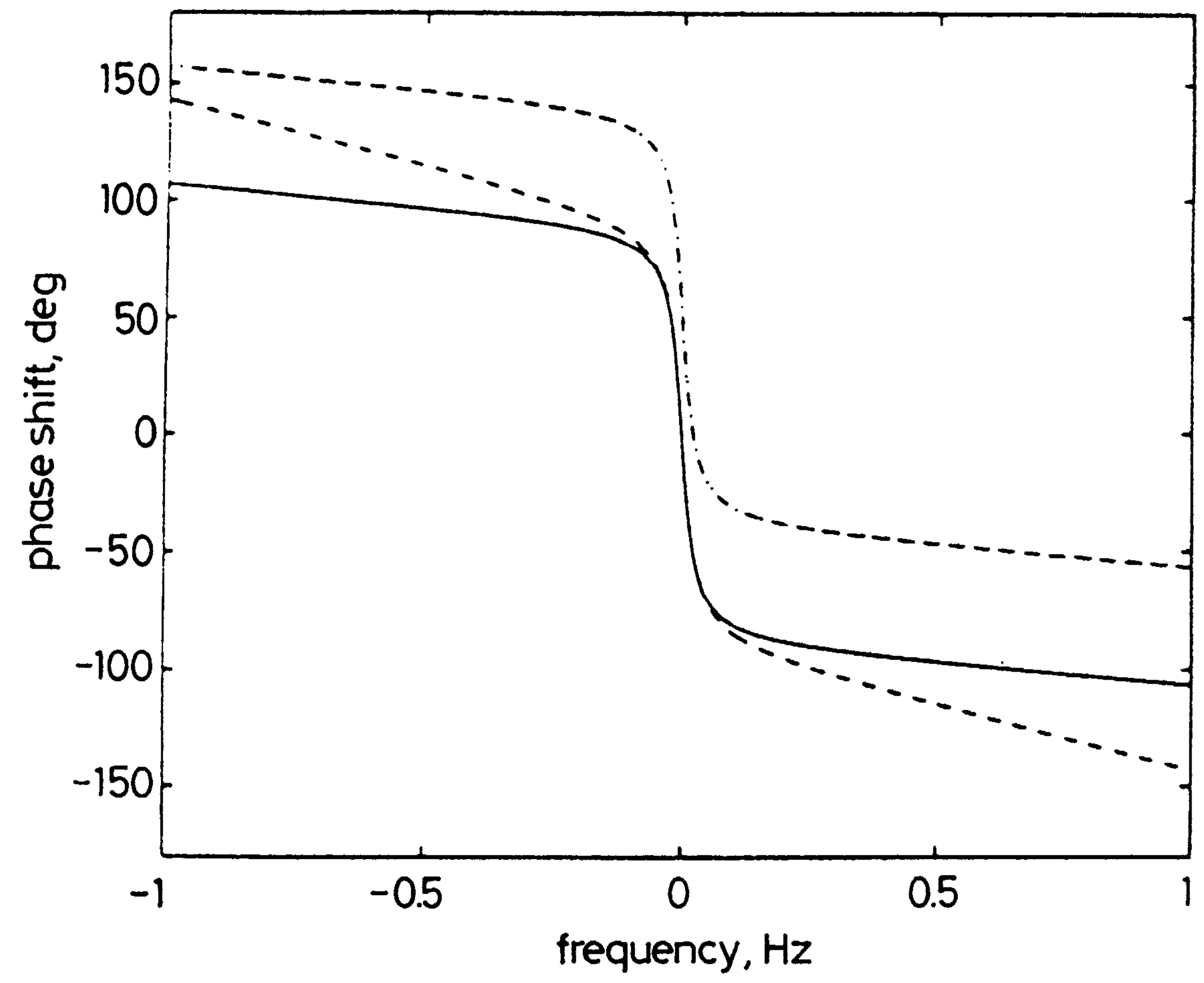

Fig. 7 *Demonstration of difference between baseband phase shift and RF phase rotation*
——— original phase response
– – – – modified phase response as a result of baseband phase shift
– · – · modified phase response as a result of RF phase rotation

Adding more delay in the transfer function effectively increases the slope of the linear phase component and hence symmetrically pushes both sides of the phase response closer to ±180°, respectively (dashed line). Delay or baseband phase shift hence directly reduces the stability of the system by subtracting away from the original phase margin of the system (pm_G).

RF phase rotation also reduces stability but in the manner shown by the dot–dashed traces. Only one side of the phase response suffers a degradation in stability (closer to +180° in this case). This degradation is equivalent to the amount of RF phase rotation imposed. Therefore, when the amount of RF phase rotation equals the original phase margin pm_G, one side of the response will have a zero phase margin, and instability will result (on that side of the spectrum).

The Figure can also explain how only a complex tone experiences the same phase shift whether it experiences an RF phase rotation or a baseband phase shift.

It is possible to have two systems with the same δm_G each having a different combination of pm_G and $|\delta|$. Both will be able to tolerate the same amount of RF phase variation since both have the same δm_G but the closed loop responses of the two systems will not be exactly the same despite the fact both have the same stability margin.

2.3 Effects of amplifier characteristics on stability II

In addition to amplifier phase variations discussed previously, the RF amplifier introduces gain variations. This directly modifies the loop gain parameter g of the MIMO model. To account for this gain change, the phase margin of $gG(s)$ must be able to be calculated as a function of g. This can be accomplished by again equating $G(s)$ to some numeric transfer function such as that given by eqn. 13.

The phase margin of $gG(s)$ is hence given by

$$pm_G = \pi + \operatorname{atan}\frac{\omega_{0dB}}{-p} - \omega_{0dB}\tau \text{ (radians)} \quad (14)$$

where:

$$\omega_{0dB} = p\sqrt{K^2g^2 - 1}\,(\mathrm{rad/s}) \qquad (15)$$

ω_{0dB} is the gain crossover frequency for controller transfer functions of the type given by eqn. 13. The gain margin can also be found by finding how much loop gain (gK) in eqn. 15 will force eqn. 14 to reduce to 0.

It is evident from the preceding therefore, that cross-coupling, as is introduced by the AM/PM distortion of the RF amplifier and error in the adjustment of δ_m (see Fig. 1) will degrade the system stability. Increases in gain as introduced by amplifier AM/AM distortion will also degrade system stability since eqns. 14 and 15 show that increases in gain reduce the phase margin and hence stability.

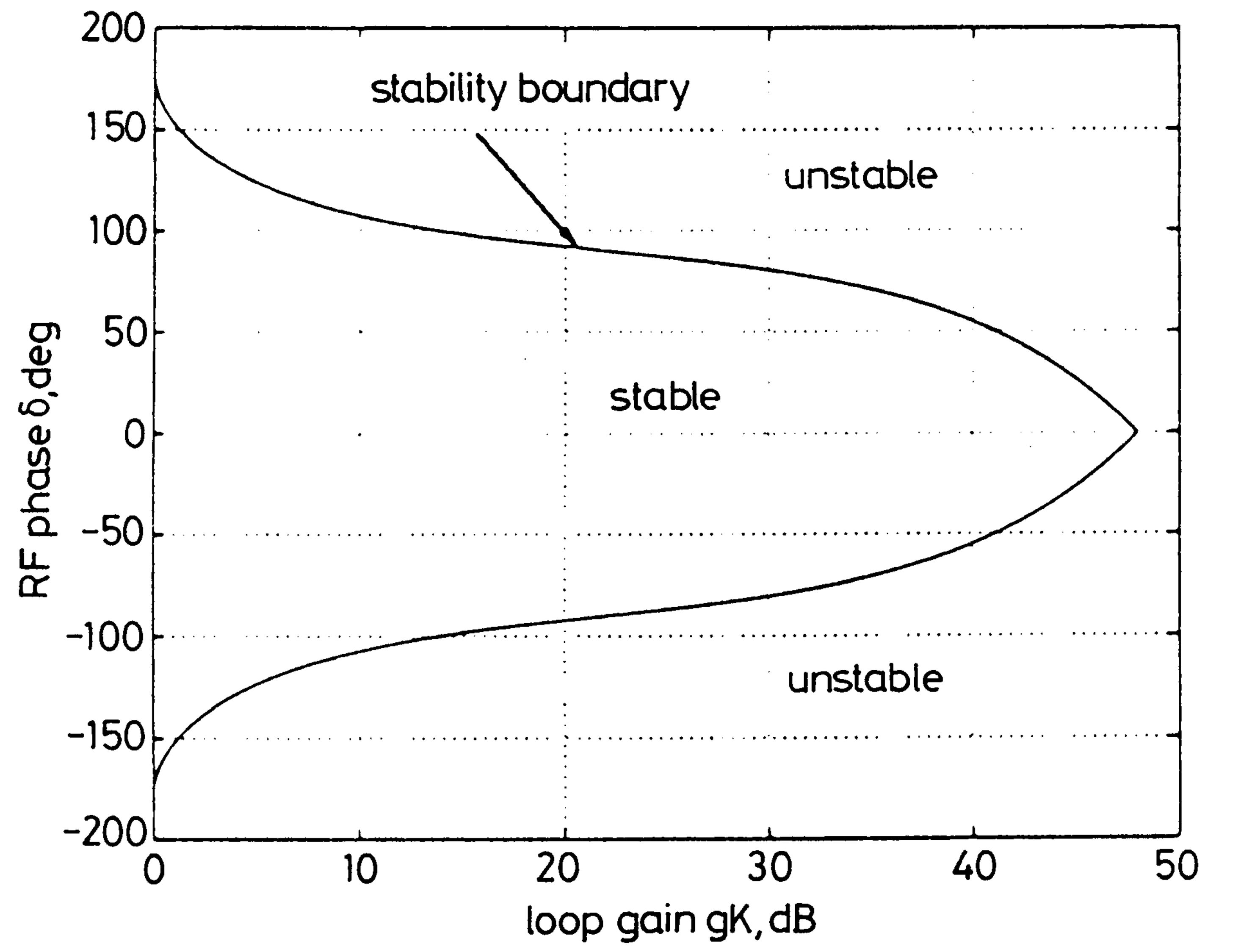

Fig. 8 *Graphical conditions for linear amplifier stability*
Stability is ensured provided amplifier operation is within the stability boundary

3 Graphical stability analysis suitable for amplifiers with weak nonlinearities

A graphical interpretation of eqn. 12 was used to form the conditions for stability as shown in Fig. 8. The stability boundary ($\delta m_G = 0$) was generated by combining eqns. 12 and 14 to give

$$|\delta| = \pi + \mathrm{atan}\frac{\omega_{0dB}}{-p} - \omega_{0dB}\tau\,(\mathrm{radians}) \qquad (16)$$

with ω_{0dB} given by eqn. 15. The delay was set to 50ns and the pole frequency was set to 126krad/s (20kHz) in eqns. 13 and 14, respectively. Within the stability boundary shown the Cartesian feedback loop is stable.

To demonstrate the use and significance of the graph the amplifier gain and phase responses of this amplifier Figs. 9–12 can be directly superimposed upon the curves of Fig. 8.

Setting the RF phase adjuster of Fig. 1 and eqn. 13, δ_m to −135°, and the DC gain (K) to 3.4dB places the amplifier traces in the position shown in Fig. 13 (a blown-up version of Fig. 8). An asterisk placed on approximately the worst stability point highlights how specific stability factors can be determined. The gain margin can be found by measuring the horizontal distance from the asterisk to the stability boundary. In other words, this distance gives the amount of additional gain the system can tolerate before instability occurs and is 2.9dB in this example. The vertical distance to the stability boundary gives the amount of RF phase rotation, which can be accommodated before instability results. This distance, is the δ margin or δm_G, and indicates 22° of RF phase rotation can be accommodated before the system becomes unstable.

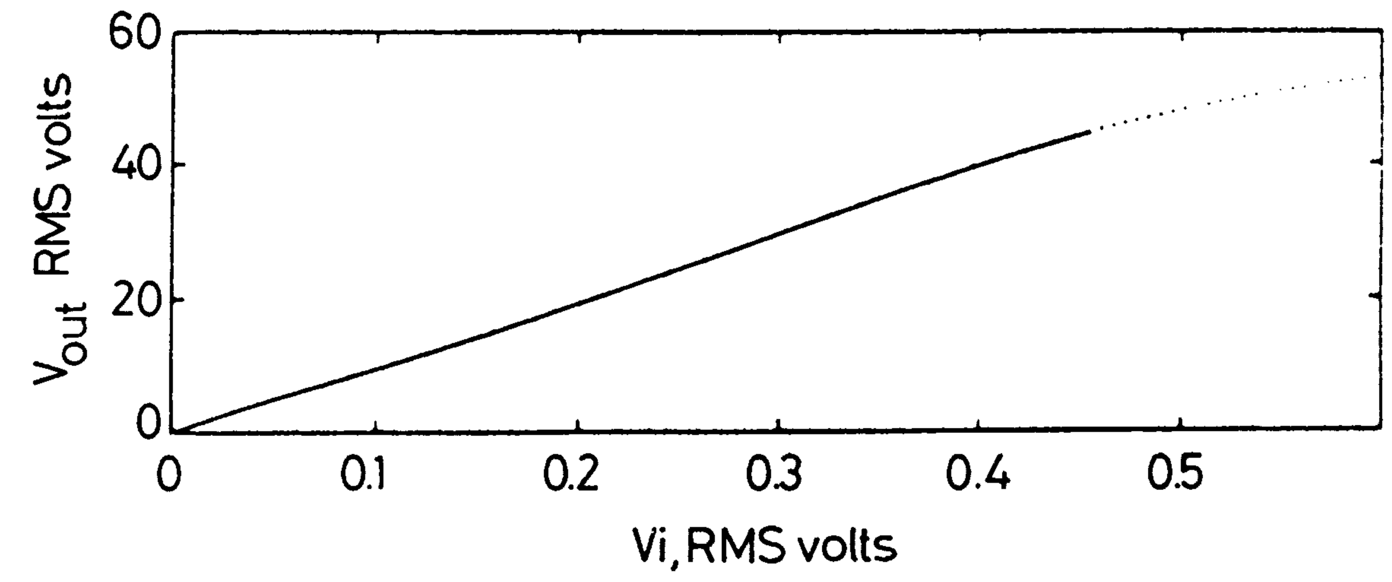

Fig. 9 *RF amplifier output voltage against input voltage*

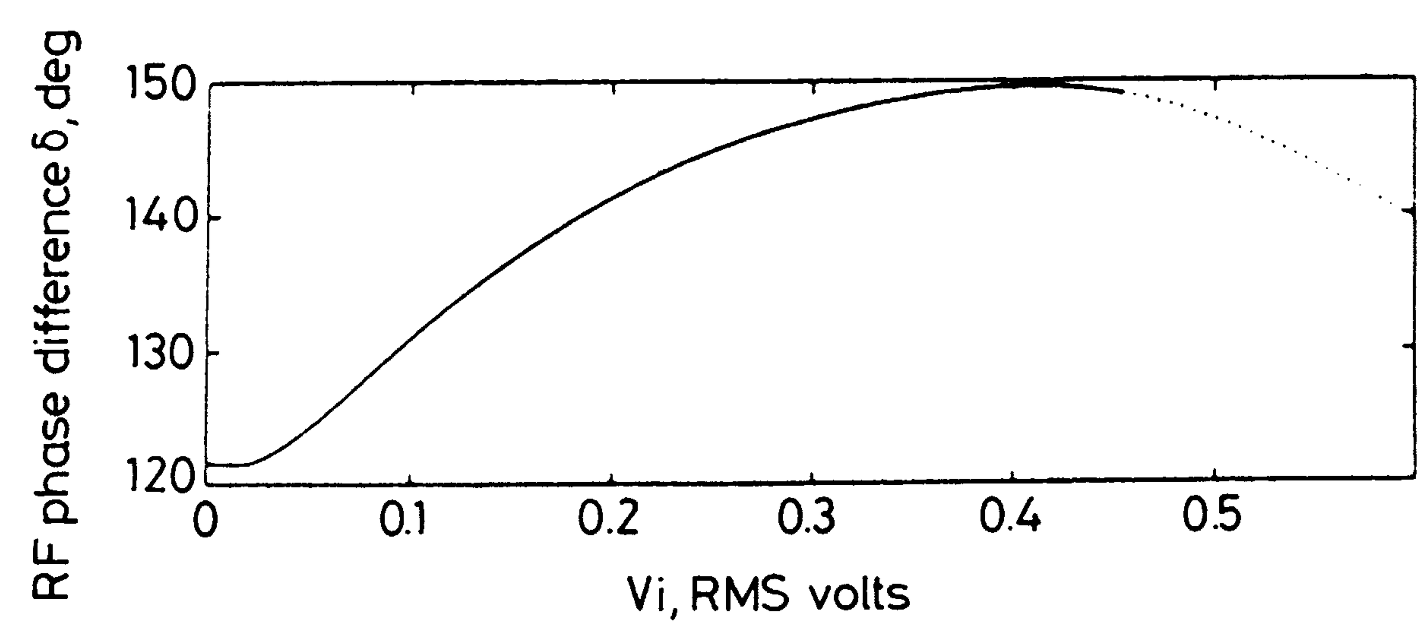

Fig. 10 *RF amplifier output phase against input voltage*

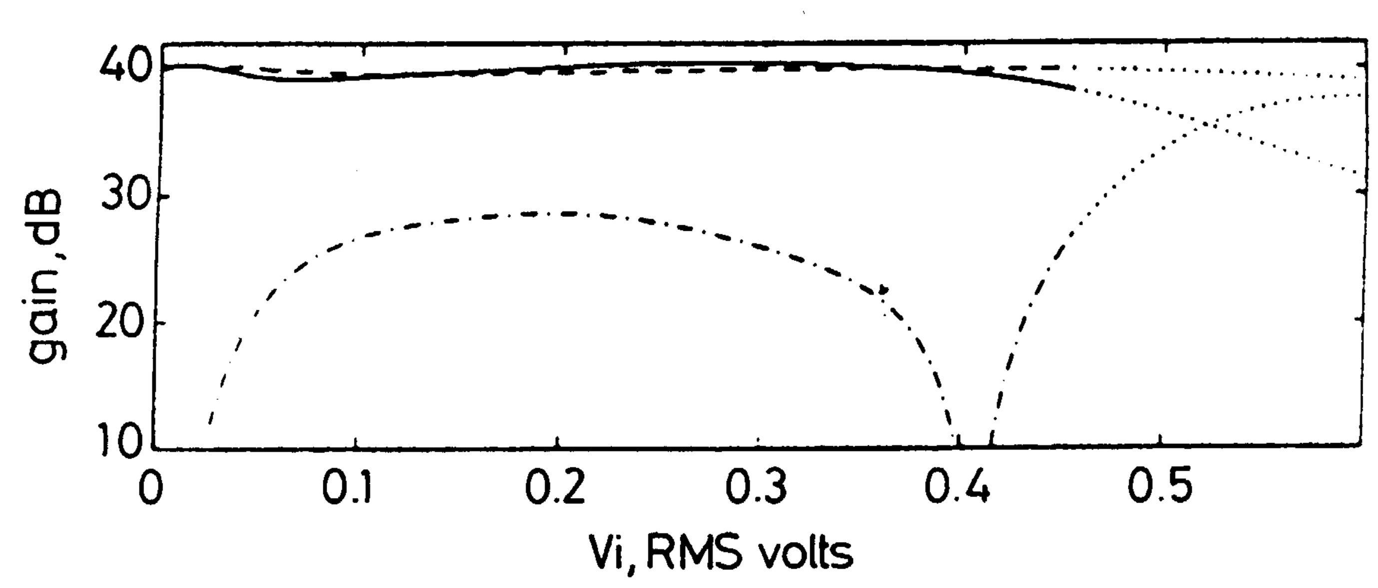

Fig. 11 *RF amplifier gains against input voltage*
——— differential gain
– – – – absolute gain
· – · – $|V_0|g_d$

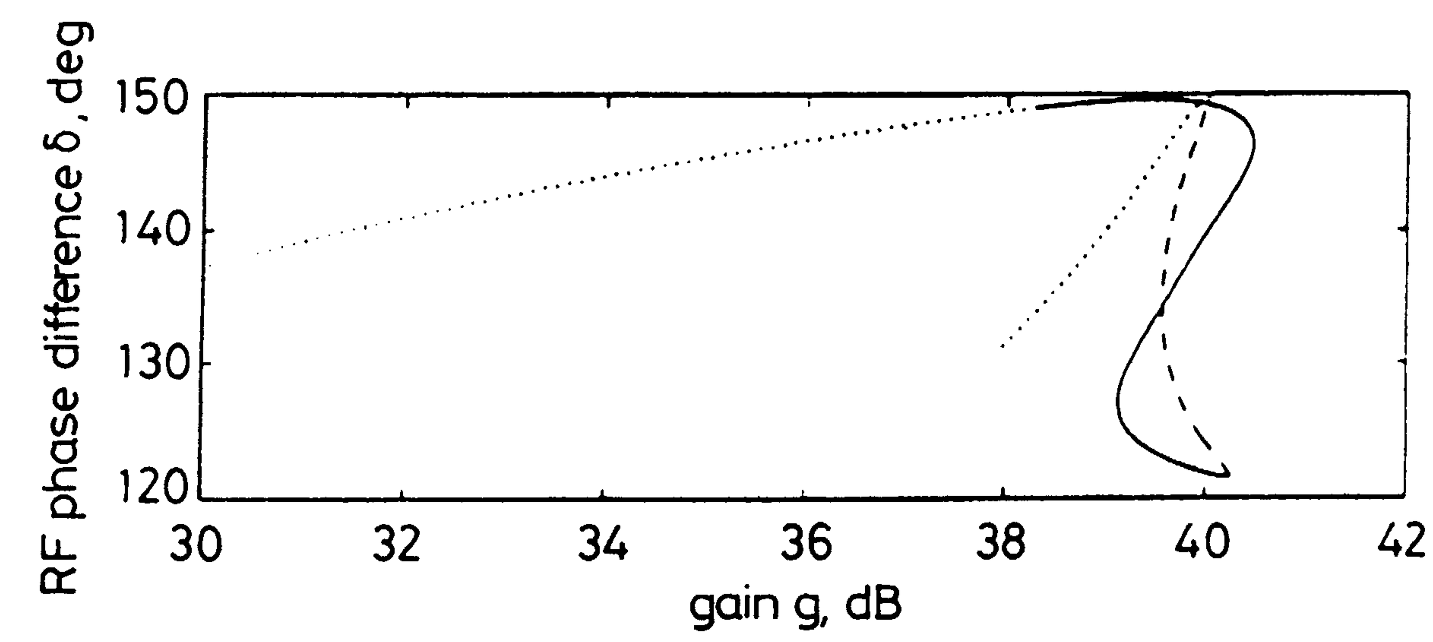

Fig. 12 *RF amplifier output phase against amplifier gain*
——— differential gain
– – – – absolute gain

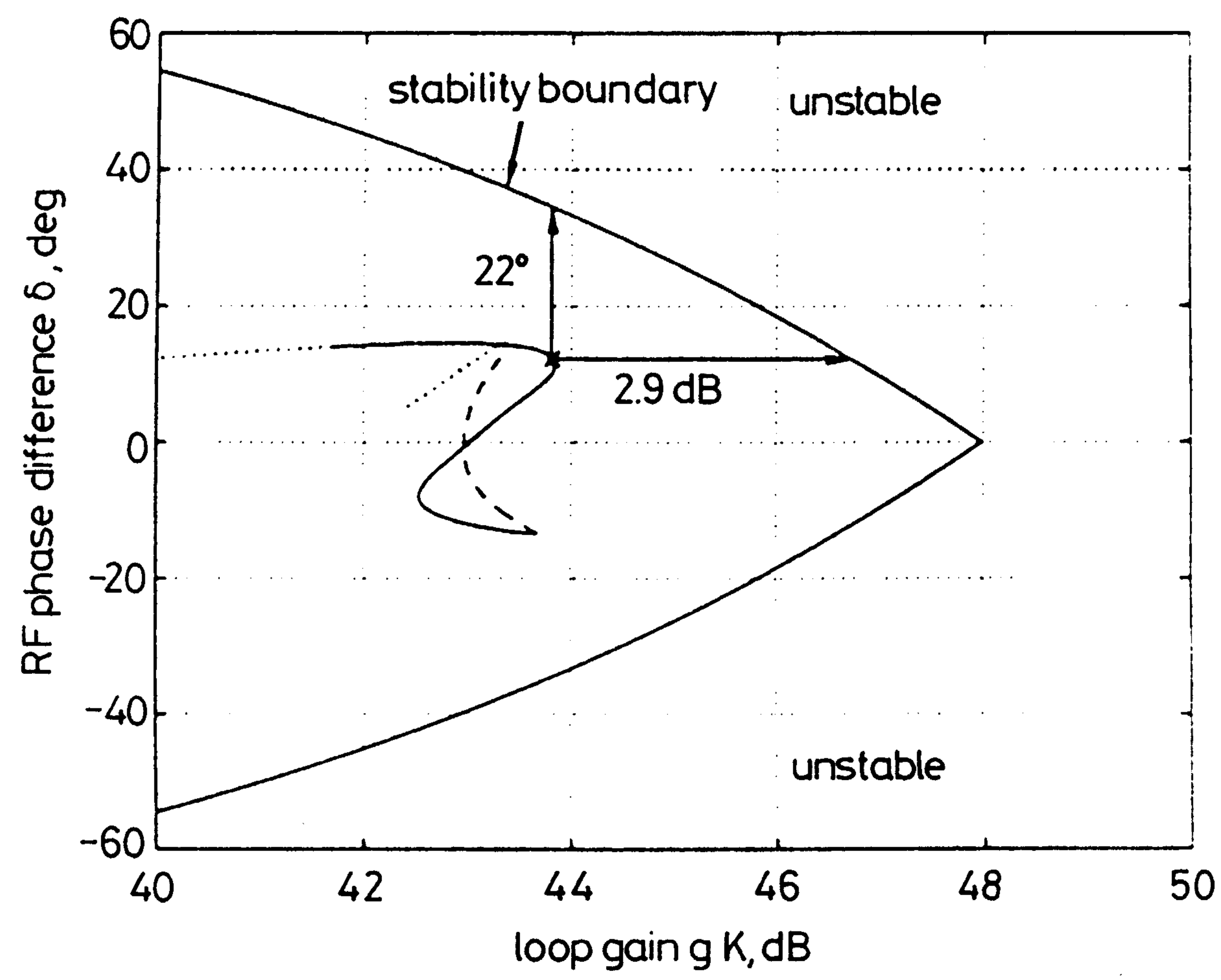

Fig. 13 *Close-up view of graphical conditions for linear amplifier stability with amplifier characteristics superimposed*
Gain and δ margins are indicated by numbered arrows

The technique is quite versatile and allows the placement of amplifier characteristics operating under different system conditions, so as δ_m is varied, the characteristics are moved in a vertical direction, and as K is varied, the characteristics are moved in a horizontal direction.

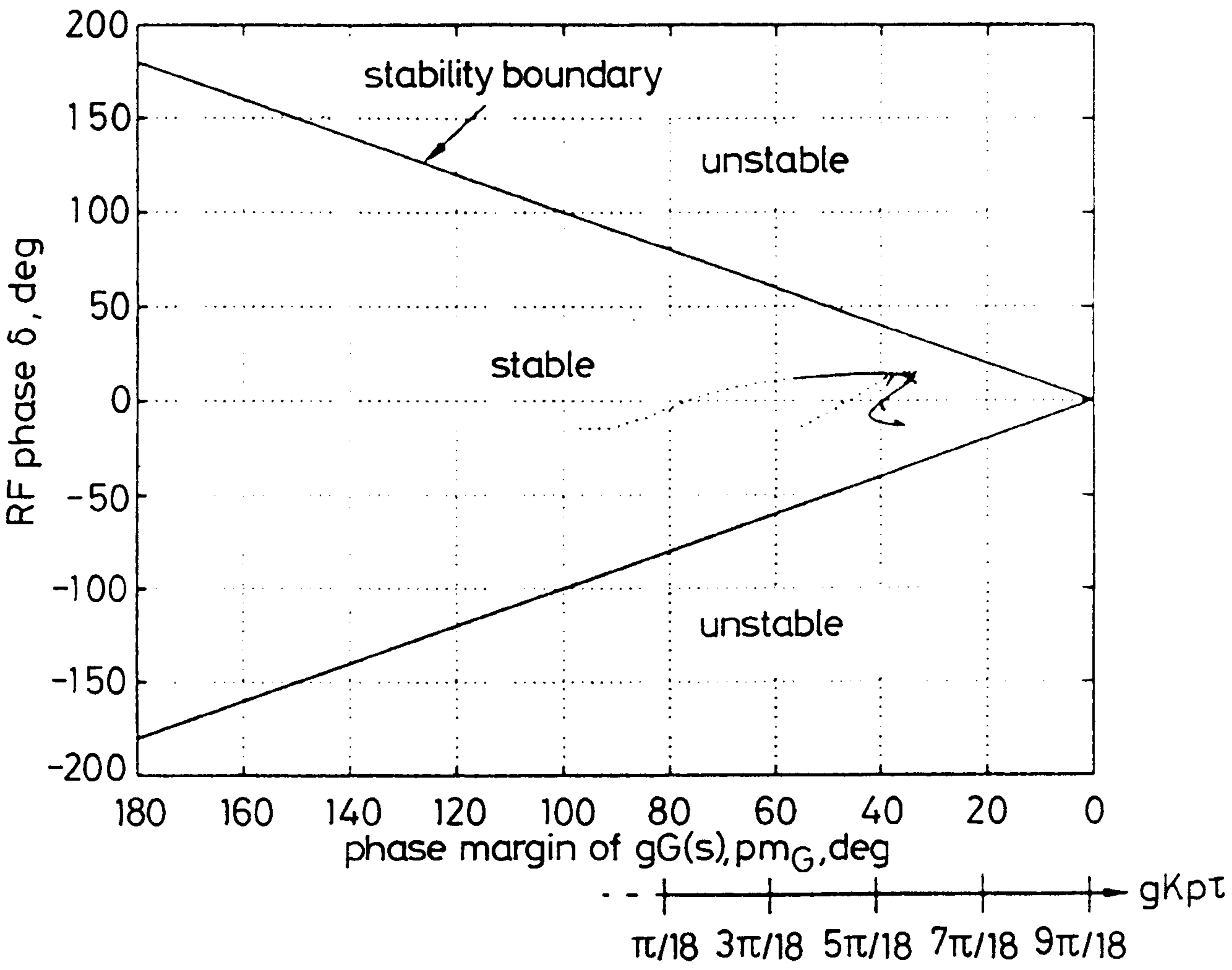

Fig. 14 *Universally applicable graphical conditions for linear amplifier stability*
Additional axis allows selection of gain, pole frequency and delay for first-order loops

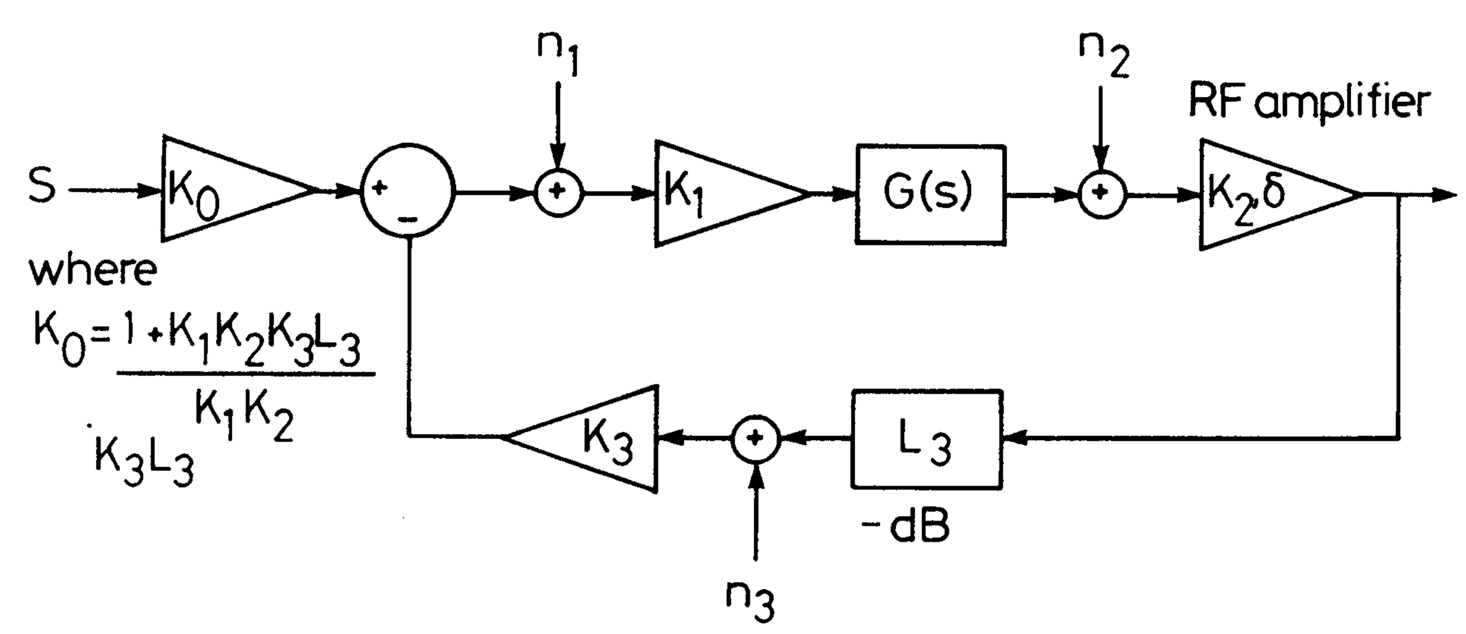

Fig. 15 *Complex noise model of Cartesian feedback loop showing distribution of loop gain and appropriate noise sources*

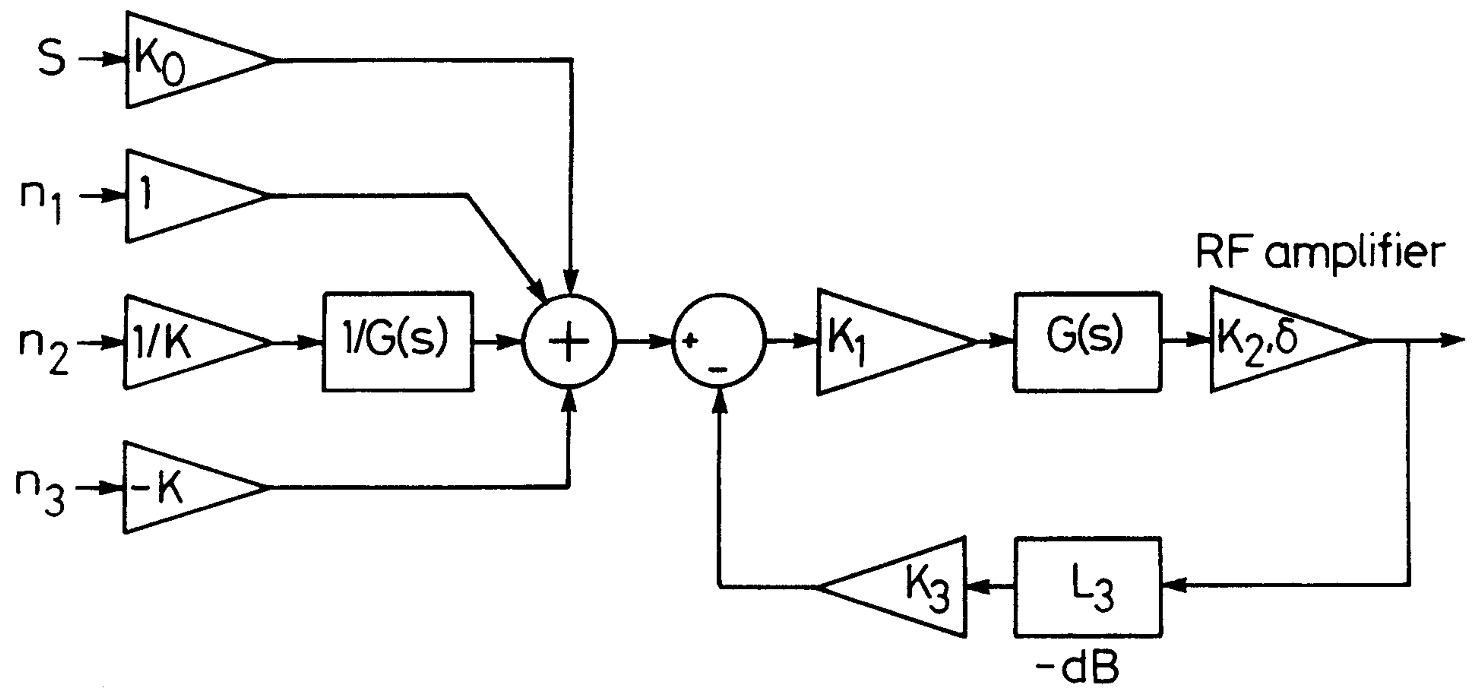

Fig. 16 *Rearranged complex noise model with noise referred to the input*

3.1 Universally applicable technique

Eqn. 12, plotted in its essential form with the amplifier characteristics superimposed is shown in Fig. 14. The graph is universally applicable because the phase margin of any transfer function (pm_G) can be applied irrespective of the nature of this transfer function (i.e. whether it contains various combinations of multiple poles and zeros, different delay and gain).

The secondary axis shown below the main graph of Fig. 14 demonstrates a simple technique by which the universal graph can be utilised. If the gain is sufficiently large for the single pole example given, eqn. 14 can be expressed by:

$$\omega_{0dB} \simeq pgK \tag{17}$$

Also, if ω_{0dB} is much greater than p, the pole will contribute $-\pi/2$ at ω_{0dB}. Eqn. 14 can thus be reduced to

$$pm_G \simeq \frac{\pi}{2} - pgK\tau \tag{18}$$

It is this expression which allows the additional axis to be drawn. Note gK in the expression and shown on the axis is not in dB.

4 Noise considerations

Although stability is an important consideration, it has been found experimentally that systems with low stability margins exhibit increased levels of out-of-band noise.

The block diagram of Fig. 15 represents a complex noise model of a Cartesian feedback system. The loop gain has been split into three components with appropriate noise sources. K_0 normalises the closed loop gain to unity. K_1 represents gain prior to the loop compensation $G(s)$ and the RF amplifier gain is represented by K_2. L_3 models the attenuation required to reduce RF feedback signals to levels appropriate for demodulation with the subsequent gain necessary represented by K_3.

This block diagram can be rearranged so that the noise can be referred back to the input (Fig. 16). At some stage, all noise sources pass through the closed loop transfer function of the Cartesian feedback loop. Setting the RF phase δ to zero, $g = 1$ and $G(s)$ with $pm_G = 30°$ (DC gain, $K = 167.7$ (44.5dB), pole frequency = 126krad/s (20kHz), and delay, $\tau = 50$ns) gives the magnitude response and phase response of Figs. 17 and 18. This response clearly demonstrates a peaking effect in the closed loop response for systems with low stability margins ($pm_G = 30°$).

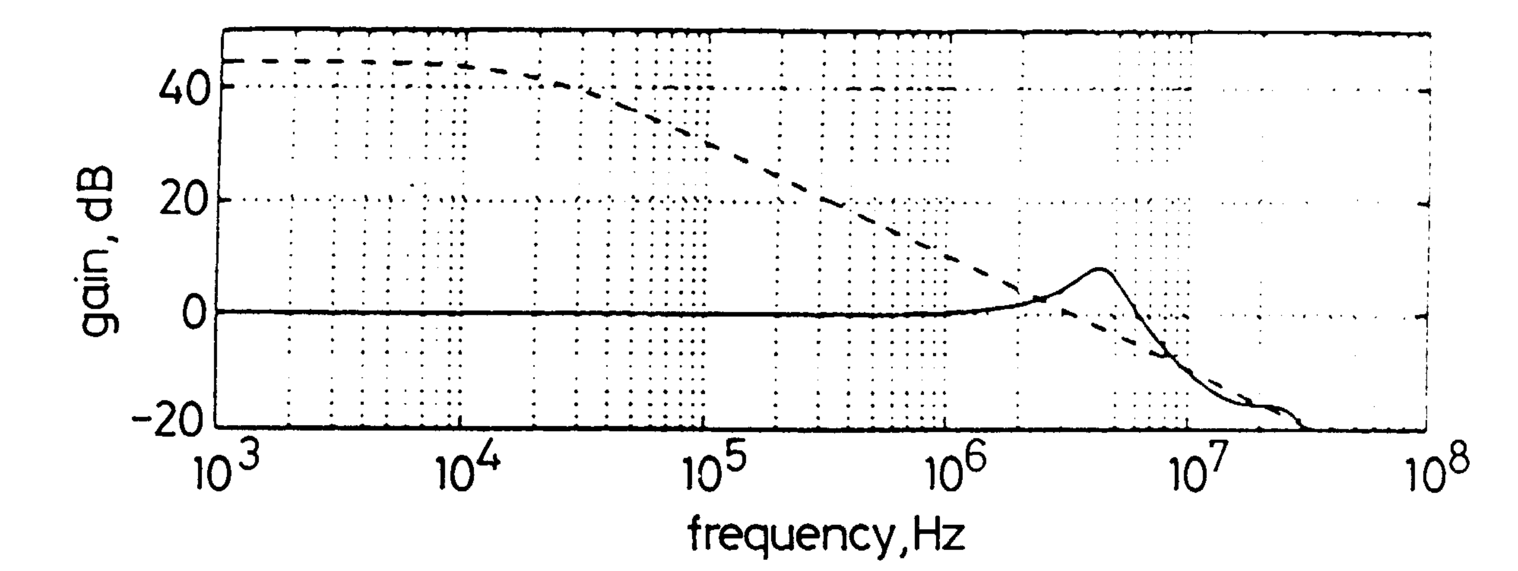

Fig. 17 *Open loop and closed loop gain responses of single pole system with delay*
- - - - open loop
——— closed loop
Amplitude peaking is evident in closed loop response

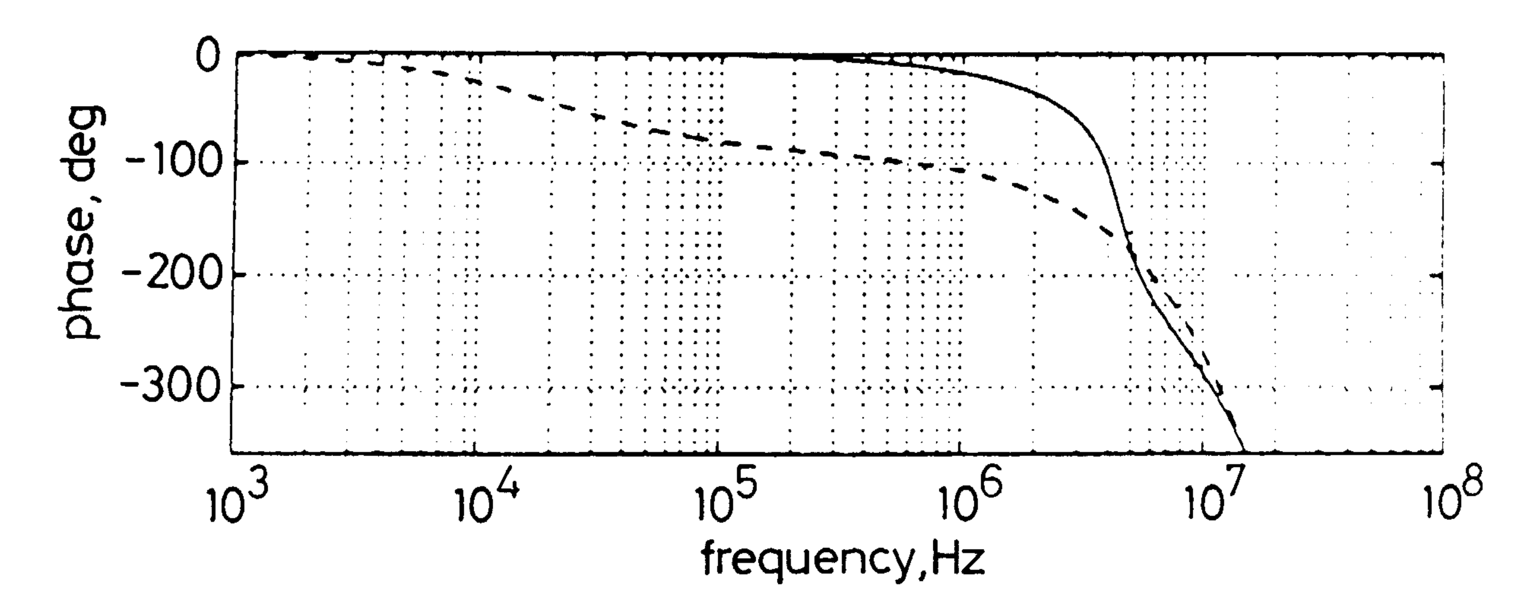

Fig. 18 *Open loop and closed loop phase responses of single pole system with delay*
- - - - open loop
——— closed loop
Amplitude peaking is evident in closed loop response

Fig. 19 shows two measured spectra of the experimental Cartesian feedback system using the class AB amplifier discussed previously. The increase in out-of-band noise is visible as peaks in the noise floor (these peaks appear broader than the solid magnitude response of Fig. 17 because a linear frequency scale is used in Fig. 19). Cartesian feedback systems should be designed to be more than just stable. There must be sufficient stability margin to limit the peaking in the out-of-band noise spectrum to a reasonable level.

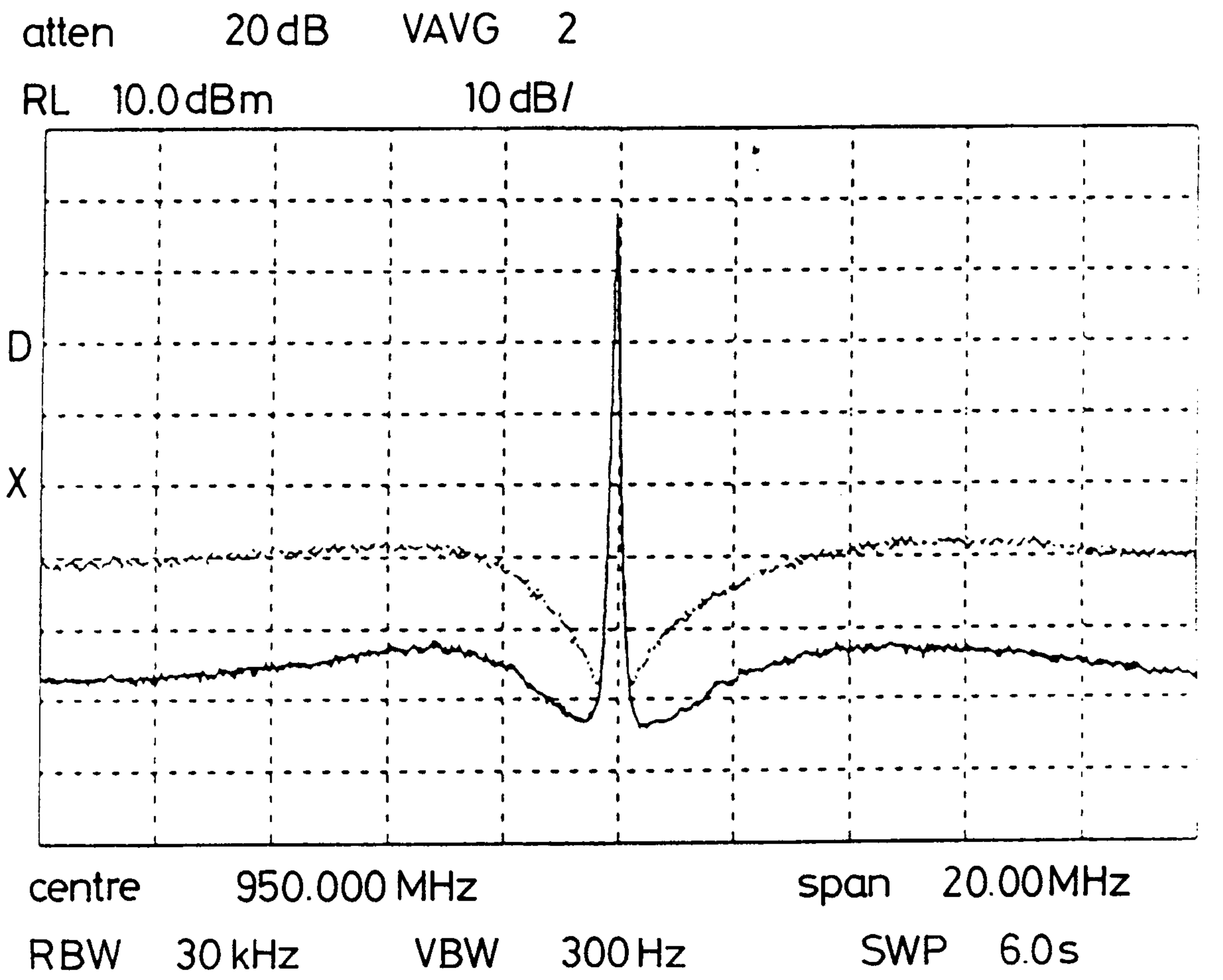

Fig. 19 *Measured wideband spectrum of Cartesian feedback transmitter*
Lighter trace (top) indicates filtering placed close to subtraction point
Darker trace (bottom) shows improved out-of-band noise performance with loop filter further up amplifier chain
Some peaking is also evident

As the stability margins of a Cartesian feedback loop are reduced either by changing δ or g, or through poor design, the out-of-band noise steadily increases. And, once the stability margins are completely consumed, high frequency oscillations will break out at a baseband frequency where the peaking in the closed loop response exists, since this frequency represents the least stable frequency of operation.

It is difficult to analyse how the noise peaking is affected exactly by changes in δ and g but it is possible to determine how the peaking is affected by the selection of $G(s)$, with $\delta = 0°$ and $g = 1$. Under these conditions the closed loop transfer function is given by

$$T(s)|_{\substack{\delta=0° \\ g=1}} = \frac{G(s)}{1+G(s)} = \frac{Kpe^{-\tau s}}{s+p+Kpe^{-\tau s}} \tag{19}$$

Now the peak of eqn. 19 occurs when the magnitude of the denominator approaches its minimum. Substituting $s = j\omega$ in the denominator gives

$$|(\text{den.})|^2 = (p + Kp\cos(\omega\tau))^2 + (\omega - Kp\sin(\omega\tau))^2 \tag{20}$$

To find the condition for no peaking, the derivative with frequency of eqn. 20 must be found and made greater than or equal to zero. Note, a rising closed loop response corresponds to a falling denominator

$$\frac{d|(\text{den.})|^2}{d\omega} = 2\omega\left(1 - \tau Kp\cos(\omega\tau) - \left(\tau^2Kp^2 + \tau Kp\right)\frac{\sin\omega\tau}{\omega\tau}\right) \tag{21}$$

Since the equation in the brackets has its minimum at $\omega = 0$:

$$\frac{d|(\text{den.})|^2}{d\omega} = 2\left(\omega - \left(\omega\tau Kp\cos(\omega\tau) + \left(\tau Kp^2 + Kp\right)\sin(\omega\tau)\right)\right) \tag{22}$$

By inspection, the derivative is positive for all values of ω if it is positive as ω tends to 0, i.e.

$$\left.\frac{d|(\text{den.})|^2}{d\omega}\right|_{\omega\to 0} \geq 0 \tag{23}$$

When peaking occurs in the closed loop magnitude response (i.e. $|T(s)|$) for a single pole system with delay, the response will always rise as the frequency is increased from zero i.e. there will never be a dip between DC and the crest of the peak.

By setting eqn. 22 to be greater than or equal to zero for small ω, the no peaking condition will be satisfied:

$$\begin{aligned} &\omega - \left(\omega\tau Kp + \left(\tau Kp^2 + Kp\right)\cdot\omega\tau\right) \geq 0 \\ &\Rightarrow \tau Kp(\tau p + 2) \leq 1 \end{aligned} \tag{24}$$

Now, since τp is usually much less than 2, the no-peaking condition can be satisfied by

$$2Kp\tau \leq 1 \tag{25}$$

For a system with a pole location of 126krad/s (20kHz) and a delay of 50ns, the nonpeaking condition would exist if the loop gain is kept below 80 (38dB) giving an open loop phase margin pm_G of 61.9° and a gain margin of 9.92dB. This is a limitation on the maximum possible distortion reduction of a Cartesian feedback system. A small degree of peaking can, however, be tolerated in which case the frequency at which the peak occurs can be found by setting the derivative of the denominator, as given by eqn. 22, to zero. The approximation $\omega \simeq 0$ is no longer valid so the Newton–Raphson numerical method for equation solving is applied giving

$$\omega_{n+1} = \omega_n - \frac{\tau Kp^2\sin\omega_n\tau + Kp\sin\omega_n\tau + w\tau Kp\cos\omega_n\tau - \omega_n}{\tau^2Kp^2\cos\omega_n\tau + 2\tau Kp\cos\omega_n\tau + \omega_n\tau^2Kp\sin\omega_n\tau - 1} \tag{26}$$

To find the position of the peak, the initial selection of ω_n must be in the vicinity of the peak. This is easily achieved since it is known that the peak will be at the least stable frequency (i.e. somewhere between the frequency at which the phase margin of $G(s)$ is calculated and the frequency at which the gain margin of $G(s)$ is calculated, as shown in Figs. 17 and 18). The frequency at which the phase margin of $G(s)$ is calculated ω_{0dB} is given in eqn. 15 and is approximately equal to Kp (with $g = 1$). Substituting Kp for ω in eqn. 26 gives a good first approximation and, following a few iterations, the frequency at which the peak occurs ω_{pk} is obtained.

Back substitution into eqn. 19 will give the magnitude of the closed loop response at the peaking frequency. The peaking with respect to the closed loop DC gain is given by

$$\begin{aligned} M_{pk} &= \frac{|T(\omega)||_{\omega=\omega_{pk}}}{|T(\omega)||_{\omega=0}} \\ &= \frac{p+Kp}{\sqrt{(p+Kp\cos\omega_{pk}\tau)^2 + (\omega_{pk} - Kp\sin\omega_{pk}\tau)^2}} \end{aligned} \tag{27}$$

For the system illustrated by Figs. 17 and 18, the peak frequency occurs at ω_{pk} = 26.95Mrad/s (4.29MHz), giving a relative peaking of M_{pk} = 2.65 (8.46dB).

It is possible to avoid the above computational effort if a rough estimate of the degree of peaking is acceptable. By definition, the phase margin is obtained when the magnitude of the open loop response is equal to one. From eqn. 19 the amount of peaking at the phase margin frequency when the loop is closed is then:

$$\begin{aligned} M_{pm} &= \frac{1\angle(pm_G - \pi)}{1 + 1\angle(pm_G - \pi)} \\ &= \frac{1}{2\sin\frac{pm_G}{2}} \end{aligned} \tag{28}$$

At the gain margin frequency, the phase of the open loop transfer function is $-\pi$. The amount of relative peaking at the gain margin frequency is then:

$$M_{gm} = \left| \frac{-1/(gm_G)}{1 - 1/(gm_G)} \right| \tag{29}$$

where g_{mG} (the gain margin) is not in dB but in linear form.

The peaking can thus be approximately determined for the system described by Figs. 15 and 16 ($p_{mG} = 30°$) giving, $M_{pm} = 1.93$ (5.72dB) and $M_{gm} = 2.02$ (6.09dB). The peaking will be greater than these factors (in this case 2–3dB), but the method still provides a reasonable qualitative estimate. Since the margins are naturally small when peaking occurs, the degree of peaking can also be qualitatively assessed by how close the amplifier characteristics are operating to the stability boundary given in Figs. 17 and 18.

From a stability point of view, the positioning of the filtering function $G(s)$ is irrelevant. From the noise point of view, however, the position of the filter can have a significant effect. When the noise sources are referred to the input as in Fig. 16 it is easy to compare the relative contribution of each noise source. At low frequencies, noise from the demodulator chain n_3 dominates since $1/G(s) \simeq 1$. At higher frequencies $1/G(s)$ rises and consequently n_2 becomes the dominant noise source. For low in-band noise K_3 must be kept small (and hence L_3 is small), and for low out-of band noise K_1 must be large (i.e. the compensation must be applied as far up the amplifier chain as possible). There are practical limitations which govern how small K_3 and K_2 can be made. K_2 represents the gain of the RF sections of the Cartesian feedback loop. There must be some gain in these circuits to enable RF power amplification. As K_2 is lowered the drive signal into the up-converting quadrature modulator is increased leading to the increased generation of intermodulation distortion. K_2 is therefore constrained by distortion considerations. Similar constraints exist on K_3. If the demodulated signals are too large, the down-converting quadrature demodulator will generate unacceptable levels of intermodulation distortion. Therefore, K_3 and hence L_3 are also constrained by distortion considerations.

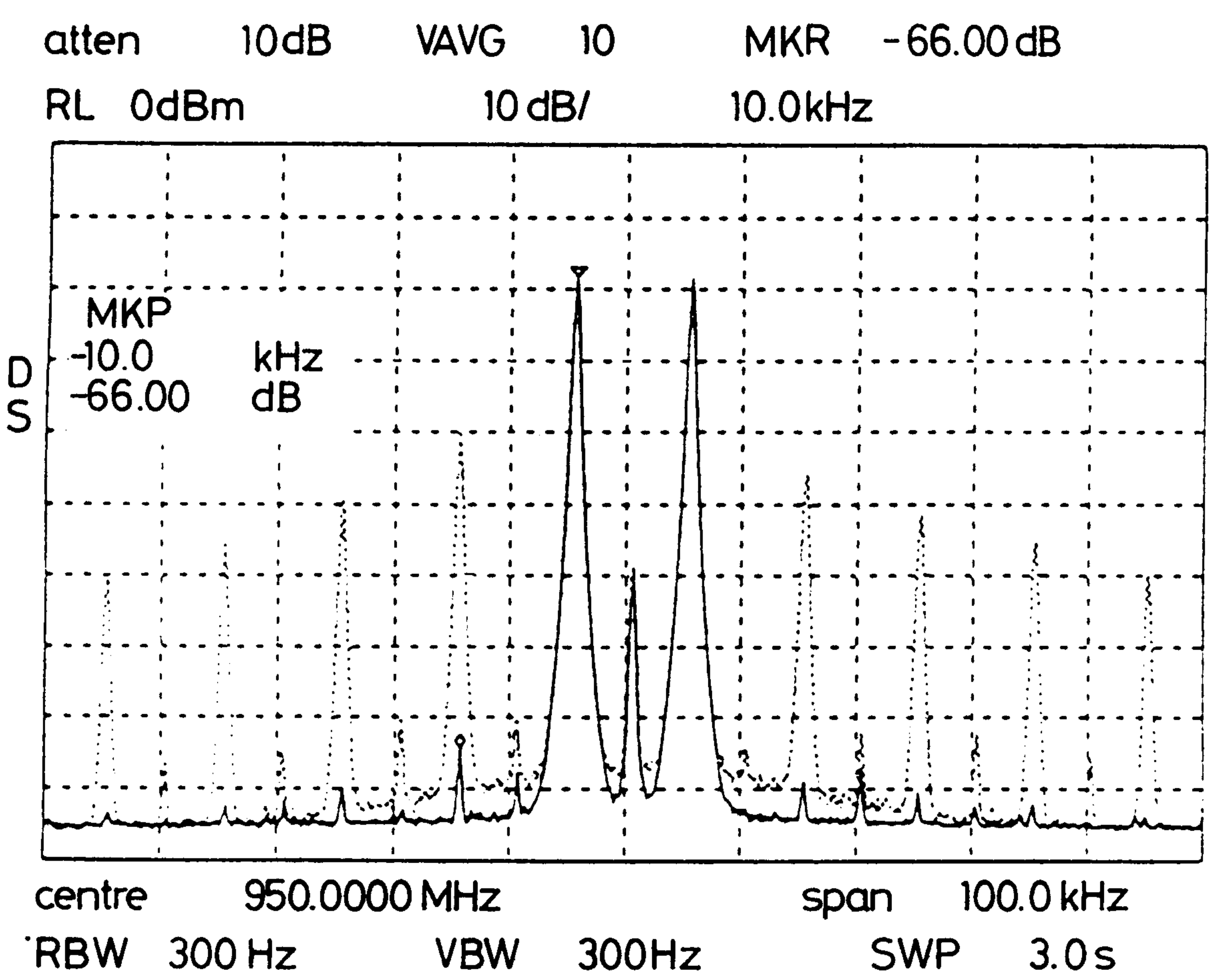

Fig.20 *Measured narrowband spectrum of Cartesian feedback transmitter*
Lighter trace indicates unlinearised open-loop two-tone test
Darker trace shows linearised closed-loop response with worst case intermodulation component 66 dB down from fundamental

The darker trace of Fig. 19 shows the improvement which can be achieved by moving the filtering away from the summation point whilst under the practical constraints described above. The lighter trace of Fig. 19 was a measurement taken with the filtering placed right after the summation point. These experimental results demonstrate the advantage of placing the filter as far away as possible from the summation point. The darker trace of Fig. 20 is a zoomed-in plot of the darker trace of Fig. 19 showing the narrowband closed-loop performance of the linearised transmitter.

5 Conclusions

The MIMO analysis presented demonstrates how RF amplifier nonlinearity, the RF phase adjuster setting, and loop gain affect the stability of the Cartesian feedback loop. It was shown that, when the amount of RF phase difference introduced by AM/PM distortion and by RF phase adjuster error equalled the system phase margin, instability resulted. The graphical technique developed from this fact demonstrates the important mechanisms which influence stability and can be utilised at the design stage, or in the practical assessment of an experimental Cartesian loop.

By basing the graph on the phase margin of the compensator, the technique can be made universally applicable irrespective of the compensation method.

Loops with low stability margins were demonstrated to exhibit closed-loop peaking. The condition of no-peaking was derived along with the degree of peaking resulting from closing a loop around a single pole with a delay. It was shown how the degree of peaking could be universally approximated by utilising the system gain and phase margins and hence determined under the influence of RF amplifier nonlinearities.

It was also concluded and demonstrated that the loop compensation should be placed as far away from the subtraction point as possible to minimise the out-of-band noise floor.

6 References

1 FAULKNER, M., and JOHANSSON, M.: 'Adaptive linearization using predistortion, experimental results', *IEEE Trans. Veh. Technol.*, 1994, **43**, (2), pp. 323–332
2 BATEMAN, A.: 'The combined analogue locked loop universal modulator (CALLUM)'. Proceedings of the 42nd IEEE vehicle technology conference, May 1992, Vol. VTC-92, pp. 759-763
3 STEWARD, R.D., and TUSUBIRA, F.F.: 'Feedforward linearisation of 950 MHz amplifiers', *IEE Proc. H*, 1988, **135**, (5), pp. 379-383
4 PETROVIC, V.: 'Reduction of spurious emission from radio transmitters by means of modulation feedback'. Proceedings of the IEE radio spectrum conservation technical conference, Sept. 1983, pp. 44-49
5 JOHANSSON, M., MATTSSON, T., SUNDSTRÖM, L., and FAULKNER, M.: 'Linearization of multi-carrier power amplifiers'. Proceedings of the 43rd IEEE vehicle technology conference, May 1993, Vol. VTC-93, pp. 684-687
6 OHISHIM, Y., MINOWA, M., FUKUDA, E., and TAKANO, T.: 'Cartesian feedback amplifier with soft landing'. Proceedings of PIMRC '92 IEEE international symposium personal indoor mobile radio communications, Oct. 1992, Vol. PMIRC-92, pp. 402-406
7 BRIFFA, M.A., and FAULKNER, M.: 'Gain and phase margins of Cartesian feedback RF amplifier linearisation', *J. Electr. Electron. Eng. Aust.*, 1994, **14**, (4), pp. 283-289